Molecular basis of dihydrouridine formation on tRNA

Futao Yu [a], Yoshikazu Tanaka [b,c], Keitaro Yamashita [a], Takeo Suzuki [d], Akiyoshi Nakamura [c], Nagisa Hirano [c], Tsutomu Suzuki [d], Min Yao [a,c], and Isao Tanaka [a,c,1]

[a]Graduate School of Life Sciences, Hokkaido University, Sapporo 060-0810, Japan
[b]Creative Research Institution 'Sousei', Hokkaido University, Sapporo 001-0021, Japan
[c]Faculty of Advanced Life Sciences, Hokkaido University, Sapporo 060-0810, Japan
[d]Department of Chemistry and Biotechnology, School of Engineering, University of Tokyo, Tokyo, 113-8656, Japan

[1]To whom correspondence should be addressed. Tel.: +81-11-706-3221; Fax: +81-11-706-4905; E-mail: tanaka@castor.sci.hokudai.ac.jp

Classification: Biological science, Biochemistry

Abstract

Dihydrouridine (D) is a highly conserved modified base found in tRNAs from all domains of life. Dihydrouridine synthase (Dus) catalyzes the D formation of tRNA through reduction of uracil base with flavin mononucleotide (FMN) as a cofactor. Here, we report the crystal structures of *Thermus thermophilus* Dus (*Tth*Dus), which is responsible for D formation at positions 20 and 20a, in complex with tRNA and with a short fragment of tRNA (D-loop). Dus interacts extensively with the D-arm and recognizes the elbow region composed of the kissing loop interaction between T- and D-loops in tRNA, pulling U20 into the catalytic center for reduction. Although distortion of the D-loop structure was observed upon binding of Dus to tRNA, the canonical D-loop/T-loop interaction was maintained. These results were consistent with the observation that Dus preferentially recognizes modified rather than unmodified tRNAs, indicating that Dus introduces D20 by monitoring the complete L-shaped structure of tRNAs. In the active site, U20 is stacked on the isoalloxazine ring of FMN, and C5 of the U20 uracil ring is covalently cross-linked to the thiol group of Cys93, implying a catalytic mechanism of D20 formation. In addition, the involvement of a cofactor molecule in uracil ring recognition was proposed. Based on a series of mutation analyses, we propose a molecular basis of tRNA recognition and D formation catalyzed by Dus.

Introduction

Posttranscriptional modification produces a diverse array of RNA molecules, and has a number of important cellular roles, such as stabilization of the RNA structure, control of translation fidelity, and metabolic response to the environment. More than 100 chemically modified nucleosides have been identified to date, the largest numbers of which are found in tRNAs. Dihydrouridine (D) modification is one of the most ubiquitous modifications of tRNA, and is found in bacteria, eukaryotes, and some archaea (1). Dihydrouridine is formed by reduction of the carbon–carbon double bond at positions 5 and 6 of the uridine base by dihydrouridine synthases (Dus), and is mostly found in the D-loop of tRNAs for which it is named. Individual tRNAs contain varying numbers of dihydrouridines. It was suggested that dihydrouridine promotes structural flexibility in RNA by destabilizing the C3'-endoribose conformation associated with base-stacked RNA (2). The content of dihydrouridine in psychrophilic organisms is significantly higher than in mesophiles and thermophiles (3). In addition, it has long been known that dihydrouridine levels are increased in cancerous tissues (4). Recently, human Dus has been reported to be involved in pulmonary carcinogenesis (5), and suggested to regulate dsRNA-activated protein kinase in cells (6).

The family of Dus has been identified in *Saccharomyces cerevisiae* and *Escherichia coli* (7, 8). Biochemical analyses showed that Dus is a flavin-dependent enzyme, which requires NADPH or NADH for its enzymatic activity. The results of genomic analyses showed that a wide number of species possess the gene encoding Dus. Moreover, several homologs of Dus genes have been found in many organisms. The four Dus from *S. cerevisiae* are responsible for reduction of uridines at specific positions, *i.e.*, Dus1 for uridine at positions 16 and 17, Dus2 for position 20, Dus3 for position 47, and Dus4 for positions 20a and 20b (7). Similarly, the site specificity and non-redundant catalytic functions were also confirmed in three Dus from *E. coli* (YjbN, YhdG, and YohI) (8). The crystal structure of Dus from *Thermotoga maritima* has been reported (9), and mutation analysis of Dus from *E. coli* revealed important residues for dihydrouridine formation (10). One of the most remarkable biochemical features of Dus is that other modifications of tRNA are required for the enzymatic activity (11). However, the details of the reaction, including the tRNA recognition mechanism and its catalysis of dihydrouridine formation, are still unknown.

In the present study, we investigated the tRNA recognition and catalytic mechanisms of Dus from a structural viewpoint. Based on the crystal structures of *Tth*Dus in complex with tRNA and tRNA fragment, and mutation analyses, we propose a tRNA recognition mechanism of Dus to discriminate modified tRNA, and a unique substrate recognition mechanism in which a cofactor molecule is used. Furthermore, the roles of each important residue in the reaction are presented.

Results

Crystal structure of Tth*Dus*

First, we determined the crystal structure of *Tth*Dus by the Se-SAD method (see methods section) at a resolution of 1.7 Å. Analogous to the Dus from *T. maritima* (9), the structure of *Tth*Dus consists of two domains, *i.e.*, an N-terminal α/β barrel domain and a helical domain (Fig. S1A). An extension of 24 residues at the C-terminus in *Tth*Dus was disordered. In addition, the region of Ala171–Ile180 located above the active site (see below) was disordered. The flavin mononucleotide (FMN) cofactor was captured at the bottom of the pocket located at the center of the N-terminal domain, indicating that this pocket is an active site. The surface including the active site formed a large positively charged groove (Fig. S1B).

Crystal structure of Tth*Dus–tRNA complex*

We recently found that *Tth*Dus expressed in *E. coli* forms a stable complex with tRNA in cells that cannot be dissociated even on SDS-PAGE (12). Rider *et al*. also reported similar results (11). In the present study, *Tth*Dus and *Tth*-$tRNA^{Phe}$ were co-expressed in *E. coli* and their complex was purified for structure analysis. Analysis of the extracted tRNA by liquid chromatography/mass spectrometry (LC/MS) showed that *Tth*-$tRNA^{Phe}$ was contained in the Dus–tRNA complex, although $tRNA^{Ile1}$, $tRNA^{Arg2}$, and $tRNA^{His}$ from *E. coli* were also detected (Fig. S2). These observations suggested that *Tth*Dus forms a complex with a variety of tRNAs regardless of the source.

The crystal structure of *Tth*Dus and *Tth*-$tRNA^{Phe}$ complex was determined by the MRSAD method at a resolution of 3.51 Å. The tRNA was captured in the positively charged groove, in which the D-, T-, and anticodon-arms are accommodated (Fig. 1A and B). The D-arm containing substrate nucleotide was recognized by both the N-terminal domain and the helical domain (Fig. 1C). The D-loop lay on the active site pocket, and bound with Asn46, Arg49, Asn90, Cys93, Ser95, Tyr103, and Arg178 in the N-terminal domain of *Tth*Dus and FMN. U20, the substrate nucleotide, flipped out from the D-loop and intruded deeply into the active site, where the base of U20 was directly recognized by Cys93, Arg178, Asn90, and FMN (Fig. 1A and C). Interestingly, the region of Ala171–Ile180, which was disordered in apo *Tth*Dus, formed a short helix and contributed to U20 recognition by hydrogen bonding using Arg178 (Fig. 1A and C). In addition, the ribose moiety of U20 was recognized by Ser95. The base and ribose moieties of G19 were recognized by Tyr103. In addition, the base of U17 was recognized by Arg49 and Asn46 through hydrogen bonding. On the other hand, the D-stem was mainly recognized by residues in the helical domain, although Asp13 and Arg14 in the N-terminal domain also contributed. The backbone structure of the T-loop was recognized by two residues in the N-terminal domain. The anticodon-arm of the tRNA was bound with residues from the helical domain and the region of Ala171–Ile180.

Conformation changes upon complex formation

Structure comparison of the bound tRNA with yeast $tRNA^{Phe}$ (PDB: 1ehz) (13) showed

remarkable conformational changes in U16 and U17 in addition to the target U20 (Fig. 2A and B). In both nucleotides, the backbone structure was distorted, and the bases turned toward different directions (Fig. 2B). U17 was recognized in a nucleotide-specific manner by Arg49 and Asn46 (Fig. 2C), whereas U16 was not (Fig. 1C). Despite the marked conformational changes on both sides, G18 and G19 still formed base pairs with U55 and C56 of the T-loop, respectively (Fig. 2B and C). In addition, G18 formed polar interactions with G57, A58, and U60, and contributed to stabilization of the elbow region. The base and ribose moieties of G19 were recognized by Tyr103. Although G18 was not directly recognized by *Tth*Dus, the backbone of C56 and G57, which interacted with G18, was recognized by Lys97 and Glu100. Therefore, G18 was recognized by *Tth*Dus through the interaction between T- and D-loops. In contrast, no significant conformational change occurred in other regions bound by *Tth*Dus, *i.e.*, the D-stem, T-loop, and anticodon-stem (Fig. 2A). These observations indicated that the distortion of U16 and U17 is independent of recognition in other regions, and is therefore caused by the flipping out of U20 to intrude into the active site.

On the other hand, the structures of *Tth*Dus and its tRNA complex were well superposed with a root mean square deviation (r.m.s.d.) of 0.57 Å for 304 Cα atoms, showing that the conformation did not change upon complexation except in the region of Ala171–Ile180.

Structure around the active site

To identify the active site structure of the tRNA complex in detail, we determined the crystal structure of *Tth*Dus in complex with a short tRNA fragment at a resolution of 1.95 Å. The structure of the RNA fragment from G18 to A21 was constructed (Fig. S3A). The target uridine was located between Cys93 and FMN cofactor with the uracil ring parallel to the isoalloxazine ring of FMN (Fig. 3). O4 and O2 of U20 formed hydrogen bonds with Nδ2 of Asn90 and Nη2 of Arg178, respectively. The relative locations of the uracil ring, FMN, and coordinating residues were similar to those of dihydroorotate dehydrogenase (DHOD) (14) and dihydropyrimidine dehydrogenase (DHPDH) (15), which also catalyze pyrimidine ring redox reaction (see Discussion) (Fig. S3C and D).

There is a space between U20 and the inner wall of the active site. A flat obvious electron density filled this space. Interestingly, this unknown molecule interacted with U20 in a manner similar to base pairing, and was surrounded by Lys132, Arg134, and His164 (Fig. 3A). Arg166 was located behind Arg134 and His164. All four of these residues are completely conserved in Dus family proteins (Fig. S4A), and were suggested to be important for the enzymatic activity (10). These residues would contribute to the reaction by recognizing U20 indirectly via this molecule. No molecules in the crystallizing buffer could be fitted to this density, suggesting that this molecule was captured in *E. coli* cells during cultivation. These observations suggest an important role of this unknown molecule as a cofactor for target base recognition.

Surprisingly, the electron density of Cys93 was connected to the C5 atom of the U20 (Fig. 3B). In addition, the coplanarity of the uridine base collapsed at the C5 and C6 atoms (Fig. 3B). These observations indicated that the C5 atom formed a covalent bond with the sulfur atom of Cys93, and consequently the double bond between C5 and C6 atoms of the uridine base was transformed into a single bond. This was supported by the results of time-of-flight

mass spectrometry (TOF-MS) analysis indicating that the molecular mass of the purified *Tth*Dus–tRNA fragment complex was 42130 Da, whereas that of apo *Tth*Dus was 39559 Da (Fig. S3B).

Identifying critical residues for tRNA complex formation

To identify the residues essential for tRNA recognition, 24 mutants were prepared and their tRNA binding activities were investigated. As Dus does not bind to transcribed tRNA (Fig. 4B), we first evaluated the interaction of each mutant with tRNA based on the presence of the covalent complex on SDS-PAGE (Fig. 4A and Fig. S5). Surprisingly, substitution of residues surrounding the unknown cofactor, *i.e.*, K132A, R134A, H164A, and R166A, resulted in complete inactivation, although they had no direct interaction with U20. In addition, N90A, C93A, and Y103A were incapable of complex formation. In contrast, R178A could form a covalent complex, although it was located in the active site and interacted with U20 directly. These results indicated the significant contribution of the cofactor to complex formation. Tyr103 interacted with the D-loop of tRNA, suggesting the importance of recognizing the elbow region for stable complex formation.

Next, to explore the contribution of the unknown cofactor, mutants surrounding the active site were prepared and their affinities were evaluated by native PAGE, in which *E. coli* $tRNA^{Arg}$ extracted from a *dus*-deficient strain of *E. coli* was used (Fig. 4B). In addition, Y103A mutant was evaluated. Complex formation was observed in the wild-type. In contrast, all mutants other than C93A showed markedly decreased binding activity (Fig. 4B). These results indicated the significant contribution of the cofactor to complex formation. In addition, N90A and Y103A were incapable of forming a complex as demonstrated on both SDS-PAGE and native PAGE, suggesting that the direct interactions of Asn90 and Tyr103 are also important. The absorption spectrum of the purified mutant protein showed that K132A did not possess FMN (Fig. S6A). As the uracil ring of U20 showed π-stacking interaction with FMN in the complex structure (Fig. 1C and 3), it is likely that FMN contributes to complex formation as well as residues surrounding the active site.

Effects of mutations on Dus activity

To discuss the roles of residues located around the active site in the enzymatic activity, the effects of mutations in these residues were evaluated. We used Dus from *E. coli* (*Ec*YjbN) for mutation analysis, as all tRNA modifications in *E. coli* have been determined. The amount of the introduced D modification in tRNA extracted from the *dus*-deficient strain of *E. coli* (*E. coli* Δ*yjbN* strain) complemented with the mutant gene was analyzed by LC/MS. *E. coli* Δ*yjbN* strain complemented with the empty vector (negative control) could introduce D modification at neither position 20 nor 20A, whereas adequate D modification was confirmed in the positive control strain complemented with the wild-type *yjbN* (Fig. 4C).

Conserved residues located around the active site were substituted with Ala, and the dihydrouridine activities were compared between mutants and wild-type (residue numbers of *Tth*Dus were used for *E. coli* mutants for clarity; the correspondences between *Tth*Dus and *Ec*YjbN are shown in Fig. S4B). Figure 4C shows the relative dihydrouridine formation activities of the mutants. K132A, C93A, and R134A showed significantly decreased activity.

As purified K132A mutant showed no absorption in the visible range, its marked inactivation could be explained by the absence of the FMN (Fig. S6B). Although weak residual activity was still observed, this was likely due to the residual FMN binding activity of K132A, which was confirmed by thermodynamic analysis of K132A (Fig. S6C). The activity of C93A was also significantly decreased, although it was not completely inhibited. However, substitution with Ser recovered the activity to a level comparable to that of the wild-type. Thus, serine and cysteine may be compatible in Dus. These results demonstrated the importance of the hydrogen atom at Cys93 as well as FMN. The activity of the R134A mutant was decreased to 31% of the wild-type, although Arg134 did not interact directly with the target nucleotide. Arg134 is located around the unknown cofactor and is one of the completely conserved residues. The decrease in activity may reflect the contribution of the unknown cofactor to the enzymatic activity as well as tRNA recognition. Although the single mutants described above demonstrated the importance of Lys132 and Cys93, each mutant still possessed weak enzymatic activity. A C93A/K132A double mutant, however, showed complete loss of activity.

Discussion

tRNA recognition mechanism of Tth*Dus*

In the structure of *Tth*Dus–tRNA complex, the D-arm, T-loop, and anticodon-stem were bound by *Tth*Dus. The conformation of the D-loop was significantly distorted upon *Tth*Dus binding (Fig. 2B), which is probably induced by the intrusion of U20 into the active site. Despite the significant conformational change at U16–U17 and U20, interactions between D- and T-loops by G18–G19 were maintained, suggesting that the structure of the elbow region was highly stabilized. The backbone structure of the elbow region was recognized in both T- and D- loops (Fig. 2C). Moreover, substitution of Tyr103, which recognized G19 stabilizing D-loop/T-loop interaction, resulted in complete incapability of complex formation (Fig. 4A and B). It should be noted that substitution of nucleotides involved in D-loop/T-loop interaction completely blocks D modification (16). These observations strongly suggest that Dus recognizes the elbow region stabilized by D-loop/T-loop interactions.

The structure of tRNA, especially in D- and T-loops, is stabilized by modifications (17). Moreover, G19–C56 base pairing is prone to disruption in the transcripts as compared to modified tRNAs (18). Several previous studies indicated that Dus targets tRNA containing modifications (11, 16). In this study, we showed that Dus can bind with tRNA that already has modifications other than D, but cannot recognize transcribed tRNA despite having the identical sequence (Fig. 4B). These observations indicated that the poor enzymatic activity for transcripts is due to the inability of complex formation. Dus should discriminate the modified tRNA in the binding process, in which the canonical structure of the D-loop/T-loop highly stabilized by the modification would be recognized. Archaeal Trm5, which targets modified tRNA, also binds tRNA in a similar manner using the elbow region as a “hallmark” (19). As both Dus and Trm5 are promiscuous enzymes that modify multiple tRNAs, this would be a

general tRNA binding mechanism to distinguish correctly modified tRNA from immature tRNAs. It is interesting to note that the proposed manner of tRNA binding is the opposite of the mechanism adopted by ArcTGT, which prefers the immature λ-form tRNA through recognition of the flexible D-loop (20).

The levels of sequence conservation of residues that interact with tRNA except U20 were remarkably low as compared to those interacting with U20. Furthermore, no conformation changes were observed in *Tth*Dus upon complex formation except for the Ala171–Ile180 region. The tRNA was captured in the positively charged groove (Fig. 1B). These observations suggest that the interaction occurs in a space-filling manner in combination with charge complementarity. The modifications in tRNA were reported to induce a conformation change of the overall L-shape structure of tRNA (21). *Tth*Dus formed a significant number of interactions with backbone structures of anticodon- and D-arms (Fig. 1C). Dus may recognize the distorted backbone structure of modified tRNA as well as the rigid D-loop/T-loop.

The high-resolution structure of *Tth*Dus–tRNA fragment complex showed the involvement of a cofactor in U20 recognition as well as FMN and directly coordinating residues, such as Asn90 (Fig. 3A). Substitution of the residues surrounding the unknown cofactor, *i.e.*, K132A, R134A, H164A, and R166A, blocked tRNA complex formation (Fig. 4A and B). However, these residues do not interact with U20 directly. In addition, a significant decrease in the enzymatic activity was observed in the R134A mutant (Fig. 4C). These residues are all completely conserved among Dus family proteins (Fig. S4A), and they have all been suggested to be important for the activity under conditions in which the expression of Dus is highly suppressed (10). These results strongly imply an important role of the unknown cofactor in U20 recognition. This can also be explained from the viewpoint of the structure. The relative orientations of the pyrimidine ring, FMN, and Cys93 are similar to those of related enzymes, DHOD and DHPDH, suggesting that the location of U20 in the structure is appropriate (Figs. S3C and D). However, the inner wall of the active site of *Tth*Dus is obviously far from the substrate. Although the substrates are directly coordinated by residues in the other two enzymes, this cannot be achieved in *Tth*Dus without the cofactor molecule. It should be noted that a sulfate ion was captured at the same position in the crystal structure of Dus from *T. maritima* (9). These structural features also emphasize the necessity of the cofactor, which is buried in the space between U20 and the completely conserved residues.

Taken together, these observations suggest that Dus recognizes the properly stabilized elbow region composed of D-loop/T-loop interaction and the distorted backbone structure of the modified tRNA, which enables Dus to discriminate between mature and immature tRNAs. At the active site, the target uridine is recognized by completely conserved residues indirectly through the unknown cofactor molecule in addition to the direct interactions by Asn90 and FMN.

Proposed reaction mechanism

Through the reaction, two hydrogen atoms in the Dus–FMN complex are transferred to C5 and C6 of the uracil ring of the target nucleotide. The arrangement of FMN and the pyrimidine ring in the *Tth*Dus–substrate complex was similar to those of DHOD and DHPDH, which catalyze similar redox reaction of pyrimidine rings. In DHOD and DHPDH, cysteine

acts as a key general-acid/base catalyst. Cys93, which is completely conserved in Dus family proteins (Fig. S4A), was located at the corresponding position in *Tth*Dus. In mutation analysis of *Ec*YjbN, alanine substitution of Cys93 caused a significant decrease in the activity, which was restored by substitution with serine. Serine was reported to be used as the catalytic residue in DHOD family 2 (22). These results showed that Cys93 is an active residue of Dus. In addition, the importance of FMN was confirmed by the marked inactivation and lack of FMN binding of K132A (Fig. 4 and Fig. S6). Taken together, these results indicated that FMN and Cys93 provide two hydrogens.

The reduced form of FMN ($FMNH_2$) can provide hydrides from two nitrogen atoms, *i.e.*, N5 and N1. The distance between C6 of U20 and N5 in FMN was 3.77 Å, which was shorter than the distance of 4.37 Å between C5 and N5 (Fig. 5A). In addition, N1 of FMN was located 4.86 Å and 5.38 Å from C5 and C6 of the pyrimidine ring, respectively, and these distances are too great to provide hydrogen. Therefore, it was concluded that the hydride is supplied from N5 of $FMNH_2$ to C6 of the pyrimidine ring. This also means that the distal hydrogen atom of Cys93 is transferred to C5. The distance between C5 of the pyrimidine ring and the sulfur atom of Cys93 is 2.05 Å, sufficiently close for hydrogen transfer. By supplying the hydride to C6 from $FMNH_2$, C5 will show nucleophilicity with the resultant electron pair. The distal hydrogen of Cys93 would be attacked by the nucleophilic electron pair of C5. As C5 does not have nucleophilicity before the hydride is provided, the reaction must start from the transfer of the hydride ion from $FMNH_2$ to C6. After transferring two hydrogen atoms, the structures of both FMN and pyrimidine ring should differ from those before the reaction, *i.e.*, the FMN and uridine adopt planar and distorted structures, respectively. These conformational changes would cause the release of product from the active site. This mechanism may be used in the step of complex formation to exclude tRNA, which already has D modification. Taken together, we propose the following reaction mechanism based on the crystal structure and the results of mutation analysis (Fig. 5B): (i) a hydride is transferred from N5 of $FMNH_2$ to C6 of the pyrimidine ring, (ii) an electron pair is consequently transferred to C5 of the pyrimidine ring, (iii) followed by nucleophilic attack by C5 to the distal hydrogen atom of Cys93, and (iv) release of the product.

The final issue to be discussed is the covalent bond formed between C5 of the uridine base and the sulfur atom in Cys93 (Fig. 3B). The reasonable configuration of functional molecules, *i.e.*, the target uridine intrudes deeply into the active site with C5 and C6 atoms adjacent to FMN and Cys93, and its similarity with the relevant enzymes, shows that the revealed structure can be considered as the structural analog of the reaction intermediate. Formation of the covalent bond with the sulfur atom suggests that a leaving group has been attached to the sulfur atom and there has been detached coupling with nucleophilic attack of the sulfate atom by the electron pair formed at C5. The substitution of the distal hydrogen atom of Cys93 into the leaving group may be caused by a non-optimal environment for the enzyme, such as temperature and redox conditions due to the heterologous overexpression. Indeed, when *Ec*YjbN was overexpressed in *E. coli*, this covalent complex was not observed (Fig. S7). Due to the covalent complex formation, we could obtain crystals and as a consequence could discuss the tRNA recognition and reaction mechanism of Dus.

Materials and Methods

Preparation of Tth*Dus,* Tth*Dus–tRNA complex, and* Tth*Dus–tRNA fragment complex*

The methods used to prepare *Tth*Dus and *Tth*Dus–tRNA complex were reported previously (12). *Tth*Dus in complex with tRNA fragment was prepared by treating *Tth*Dus–tRNA complex with RNaseA (Sigma-Aldrich) followed by purification by Ni affinity chromatography and size exclusion chromatography. Full details of the purification procedures are presented in the SI Appendix.

Crystallization and data collection

Crystallization and data collection of SeMet-labeled *Tth*Dus, native *Tth*Dus, and *Tth*Dus–tRNA complex were reported previously (12). The crystals of *Tth*Dus–tRNA fragment complex were obtained from buffer containing 0.1 M HEPES (pH 7.0) and 18% (w/v) PEG 12000. The X-ray diffraction data set was collected at beamline BL-5A of Photon Factory (Tsukuba, Japan).

Structure determination and refinement

The structure of *Tth*Dus was determined at a resolution of 1.70 Å by the Se-SAD method. The crystal structure of *Tth*Dus in complex with *Tth*-tRNA^{Phe} was determined at a resolution of 3.51 Å by the MRSAD method using the structure of *Tth*Dus as a search model and Se atoms as anomalous scatterers. The crystal structure of the *Tth*Dus–tRNA fragment complex was determined at 1.95 Å resolution by the molecular replacement method using the structure of *Tth*Dus as a search model. The statistics for data collection and refinement are shown in Table S1. The details of the structure determination procedures are presented in the SI Appendix.

Confirmation of covalent complex formation for Tth*Dus mutants by SDS-PAGE*

*Tth*Dus mutants and *Tth*-tRNA^{Phe} were coexpressed in *E. coli* strain B834(DE3). The expressed Dus mutants were purified from the soluble fraction after heat treatment at 70°C for 20 min by Ni Sepharose 6 Fast Flow (GE Healthcare). The concentration of *Tth*Dus mutant was determined using a Quant-iT Protein Assay Kit (Invitrogen), and adjusted to 0.13 mg mL^{-1}. Aliquots of 6 μL of the samples were subjected to SDS-PAGE. All vectors for mutation analyses were prepared with a KOD-Plus Mutagenesis Kit (Toyobo).

Gel shift assay

Gel shift assay was performed as described previously (23).

Evaluation of dihydrouridine formation in tRNA by E. coli *yjbN*

The wild-type and mutant *yjbN*-pMW118 (Nippon Gene) vector was used to complement the *E.coli yjbN* knockout strain (*E. coli ΔyjbN*). The extracted total tRNA from cells was digested with RNase T1, and then analyzed by capillary liquid chromatography nano-electrospray ionization/mass spectrometry (24). Among the fragments obtained from total tRNA by RNase

T1 treatment, the ADAGp fragment derived from D-loops of $tRNA^{Arg2}$ and $tRNA^{Arg3}$ were used to estimate the amount of introduced dihydrouridine. The fraction of introduced dihydrouridine was estimated from the relative amounts of ADAGp and AUAGp fragments. The rates of the individual mutants were compared with that of the wild-type enzyme. The details are described in the SI Appendix.

Acknowledgments

We thank Dr. Kenjyo Miyauchi for his support in preparation of $tRNA^{Arg2}$. This work was supported by Grants-in-Aid from the Ministry of Education, Science, Sports, and Culture of Japan (Y.T., I.T., and M.Y.). F.Y. was supported by the International Graduate Program for Research Pioneers in Life Sciences (IGP-RPLS).

FOOTNOTES

Data deposition: The atomic coordinates of *Tth*Dus, *Tth*Dus–tRNA fragment complex, and *Tth*Dus–tRNA complex have been deposited in the Protein Data Bank with the accession numbers 3B0P, 3B0U, and 3B0V, respectively.

FIGURE LEGENDS

Figure 1. Overall structure of *Tth*Dus–tRNA complex (A) Ribbon diagram. The region of Ala171–Ile180, which was disordered in the RNA-free *Tth*Dus, is shown in red. FMN is shown as sticks. **(B)** Electrostatic surface potential of *Tth*Dus. Positively and negatively charged surfaces are colored blue and red, respectively ($\pm 5\ k_bTe_c^{-1}$). **(C)** Overall interaction scheme among *Tth*Dus, FMN, and tRNA. Hydrogen bonds, π-stacking interaction, and covalent bond between *Tth*Dus and tRNA are shown as black, green, and red arrows, respectively.

Figure 2. T- and D-loop recognition mechanisms (A) Conformational differences between the bound *Tth*-$tRNA^{Phe}$ and yeast $tRNA^{Phe}$. The cartoon model is colored according to the r.m.s.d. between two tRNA molecules from blue (0.59 Å) to red (6.49 Å). All atoms in the ribose and phosphate moieties were used for calculation. *Tth*Dus is shown as a white surface. **(B)** Superposition of the T-arms and D-loops of *Tth*-$tRNA^{Phe}$ (red) and yeast $tRNA^{Phe}$ (blue). The numbers represent the tRNA base positions. **(C)** Recognition of the elbow region. Polar interactions between *Tth*Dus residues and tRNA nucleotides (red dashed line) and those within tRNA nucleotides (yellow dashed line) are shown as stereo views. The cartoon models of *Tth*Dus and tRNA are also shown in orange and green, respectively.

Figure 3. Structure of *Tth*Dus–tRNA fragment complex. (A) Close-up view of the U20 binding site (stereo views). Electron density (Fo-Fc map) of the unknown cofactor molecule is also shown as green mesh (contoured at 3σ). Dotted lines represent hydrogen bonds. Water molecule is shown as a red ball. **(B)** Covalent bond between Cys93 and U20. The 2Fo-Fc map is also shown (contoured at 2σ).

Figure 4. Mutation analyses (A) Evaluation of the covalent complex formation of *Tth*Dus mutants by SDS-PAGE. Results for the mutants in the active site are shown. The results for the Y103A mutant, which cannot form a covalent complex, are also shown. Other mutants are shown in Supplementary Figure S5. **(B)** Native PAGE of the *Tth*Dus mutants incubated with $tRNA^{Arg}$ extracted from *E. coli dus*-deficient strain. The results for wild-type with transcribed $tRNA^{Arg}$ are also shown. Lane 1: 20 pmol tRNA, lane 2; 20 pmol tRNA + 20 pmol *Tth*Dus mutant, lane 3; 20 pmol tRNA + 40 pmol *Tth*Dus mutant, lane 4; 20 pmol tRNA + 60 pmol *Tth*Dus mutant. **(C)** Enzymatic activity of each *Ec*YjbN mutant. The amounts of dihydrouridine introduced into *E. coli* $tRNA^{Arg2}$ and $tRNA^{Arg3}$ are shown relative to the wild-type.

Figure 5. Proposed reaction mechanism of Dus (A) Distances between Cys93, target U20, and FMN in the structure of *Tth*Dus–tRNA fragment complex. **(B)** Schematic representation of proposed mechanism for uridine reduction of Dus. Hydride attacks C6 of uridine with a slight positive charge (left). The generated electron pair at C5 attacks the distal hydrogen of Cys93 (center). Dihydrouridine is generated (right).

REFERENCES

1. Sprinzl M, Horn C, Brown M, Ioudovitch A, Steinberg S (1998) Compilation of tRNA sequences and sequences of tRNA genes. *Nucleic Acids Res.* 26:148-153.
2. Dalluge JJ, Hashizume T, Sopchik AE, McCloskey JA, Davis DR (1996) Conformational flexibility in RNA: the role of dihydrouridine. *Nucleic Acids Res.* 24:1073-1079.
3. Dalluge JJ, et al. (1997) Posttranscriptional modification of tRNA in psychrophilic bacteria. *J. Bacteriol.* 179:1918-1923.
4. Kuchino Y, Borek E (1978) Tumour-specific phenylalanine tRNA contains two supernumerary methylated bases. *Nature* 271:126-129.
5. Kato T, et al. (2005) A novel human tRNA-dihydrouridine synthase involved in pulmonary carcinogenesis. *Cancer Res.* 65:5638-5646.
6. Mittelstadt M, et al. (2008) Interaction of human tRNA-dihydrouridine synthase-2 with interferon-induced protein kinase PKR. *Nucleic Acids Res.* 36:998-1008.

7. Xing F, Hiley SL, Hughes TR, Phizicky EM (2004) The specificities of four yeast dihydrouridine synthases for cytoplasmic tRNAs. *J. Biol. Chem.* 279:17850-17860.
8. Bishop AC, Xu J, Johnson RC, Schimmel P, de Crécy-Lagard V (2002) Identification of the tRNA-dihydrouridine synthase family. *J. Biol. Chem.* 277:25090-25095.
9. Park F, et al. (2004) The 1.59 Å resolution crystal structure of TM0096, a flavin mononucleotide binding protein from *Thermotoga maritima*. *Proteins* 55:772-774.
10. Savage DF, de Crécy-Lagard V, Bishop AC (2006) Molecular determinants of dihydrouridine synthase activity. *FEBS Lett.* 580:5198-5202.
11. Rider LW, Ottosen MB, Gattis SG, Palfey BA (2009) Mechanism of dihydrouridine synthase 2 from yeast and the importance of modifications for efficient tRNA reduction. *J. Biol. Chem.* 284:10324-10333.
12. Yu F, et al. (2011) Crystallization and preliminary X-ray crystallographic analysis of dihydrouridine synthase from *Thermus thermophilus* and its complex with tRNA. *Acta Crystallogr. Sect. F Struct. Biol. Cryst. Commun.* 67:685-688.
13. Shi H, Moore PB (2000) The crystal structure of yeast phenylalanine tRNA at 1.93 Å resolution: a classic structure revisited. *RNA* 6:1091-1105.
14. Rowland P, Björnberg O, Nielsen FS, Jensen KF, Larsen S (1998) The crystal structure of *Lactococcus lactis* dihydroorotate dehydrogenase A complexed with the enzyme reaction product throws light on its enzymatic function. *Protein Sci.* 7:1269-1279.
15. Dobritzsch D, Schneider G, Schnackerz KD, Lindqvist Y (2001) Crystal structure of dihydropyrimidine dehydrogenase, a major determinant of the pharmacokinetics of the anti-cancer drug 5-fluorouracil. *EMBO J.* 20:650-660.
16. Cavaille J, Chetouani F, Bachellerie JP (1999) The yeast Saccharomyces cerevisiae YDL112w ORF encodes the putative 2'-O-ribose methyltransferase catalyzing the formation of Gm18 in tRNAs. *RNA* 5:66-81.
17. Derrick WB, Horowitz J (1993) Probing structural differences between native and in vitro transcribed Escherichia coli valine transfer RNA: evidence for stable base modification-dependent conformers. *Nucleic Acids Res.* 21:4948-4953.
18. Perret V, et al. (1990) Conformation in solution of yeast tRNA(Asp) transcripts deprived of modified nucleotides. *Biochimie* 72:735-743.
19. Goto-Ito S, Ito T, Kuratani M, Bessho Y, Yokoyama S (2009) Tertiary structure checkpoint at anticodon loop modification in tRNA functional maturation. *Nat. Struct. Mol. Biol.* 16:1109-1115.
20. Ishitani R, et al. (2003) Alternative tertiary structure of tRNA for recognition by a posttranscriptional modification enzyme. *Cell* 113:383-394.
21. Byrne RT, Konevega AL, Rodnina MV, Antson AA (2010) The crystal structure of unmodified $tRNA^{Phe}$ from *Escherichia coli*. *Nucleic Acids Res.* 38:4154-4162.
22. Björnberg O, Jordan DB, Palfey BA, Jensen KF (2001) Dihydrooxonate is a substrate of dihydroorotate dehydrogenase (DHOD) providing evidence for involvement of cysteine and serine residues in base catalysis. *Arch. Biochem. Biophys.* 391:286-294.
23. Nakamura A, Yao M, Chimnaronk S, Sakai N, Tanaka I (2006) Ammonia channel couples glutaminase with transamidase reactions in GatCAB. *Science* 312:1954-1958.
24. Suzuki T, Ikeuchi Y, Noma A, Suzuki T, Sakaguchi Y (2007) Mass spectrometric

identification and characterization of RNA-modifying enzymes. *Methods Enzymol.* 425:212-229.

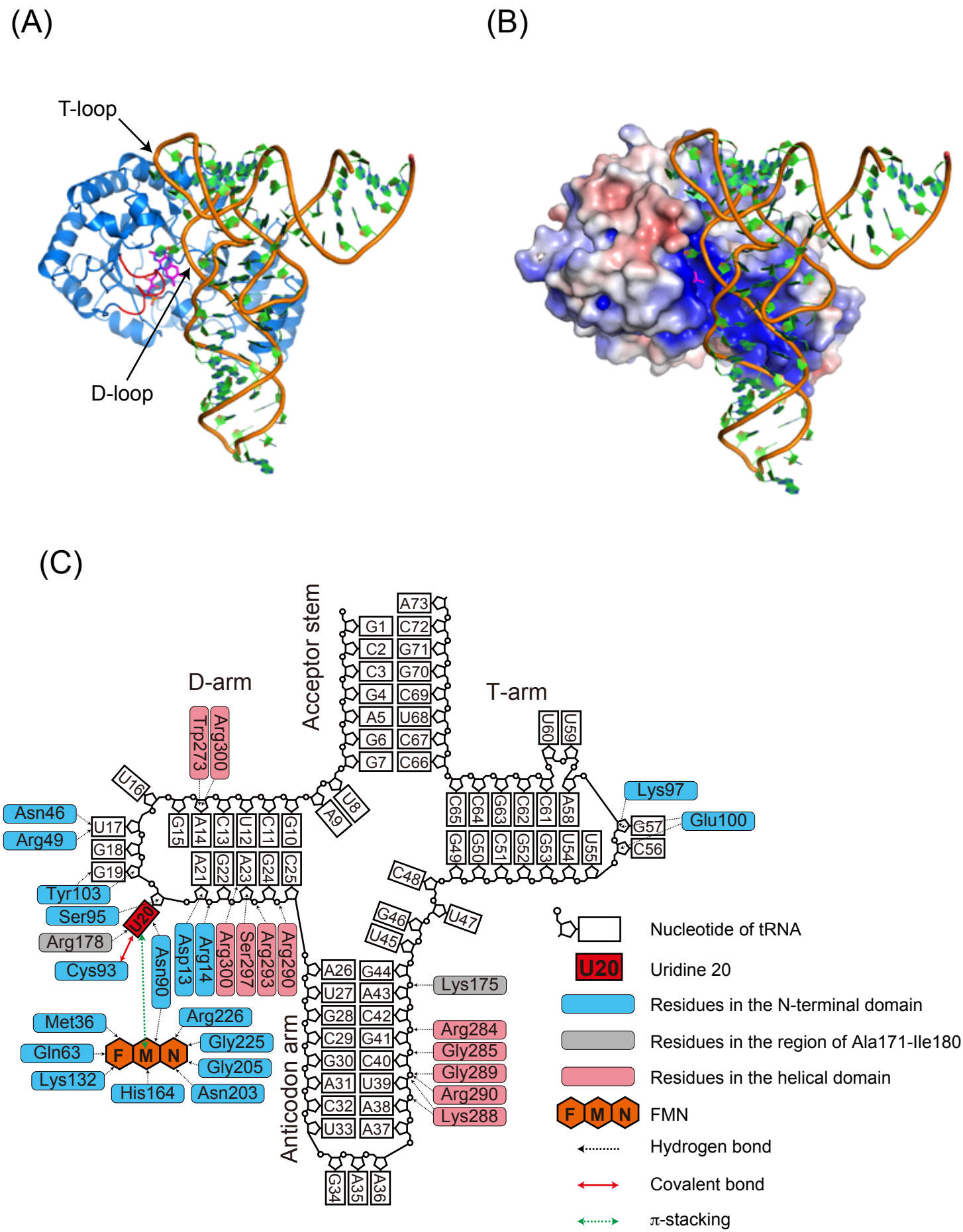
(A)
T-loop
D-loop
(B)
(C)
D-arm
Acceptor stem
T-arm
Anticodon arm
Trp273
Arg300
U16
U8
A9
A73
G1
C72
C2
G71
C3
G70
G4
C69
A5
U68
G6
C67
G7
C66
U60
U59
Lys97
Glu100
G57
C56
C65
C64
G63
C62
C61
A58
G49
G50
C51
G52
G53
U54
U55
C48
G46
U45
U47
Asn46
Arg49
U17
G18
G19
G15
A14
C13
U12
C11
G10
A21
G22
A23
G24
C25
Tyr103
Ser95
Arg178
Cys93
U20
Asn90
Asp13
Arg14
Arg300
Ser297
Arg293
Arg290
A26
G44
U27
A43
G28
C42
C29
G41
G30
C40
A31
U39
C32
A38
U33
A37
G34
A35
A36
Lys175
Arg284
Gly285
Gly289
Arg290
Lys288
Met36
Gln63
Lys132
Arg226
Gly225
Gly205
His164
Asn203
F
M
N
Nucleotide of tRNA
U20
Uridine 20
Residues in the N-terminal domain
Residues in the region of Ala171-Ile180
Residues in the helical domain
FMN
Hydrogen bond
Covalent bond
π-stacking

Figure 1

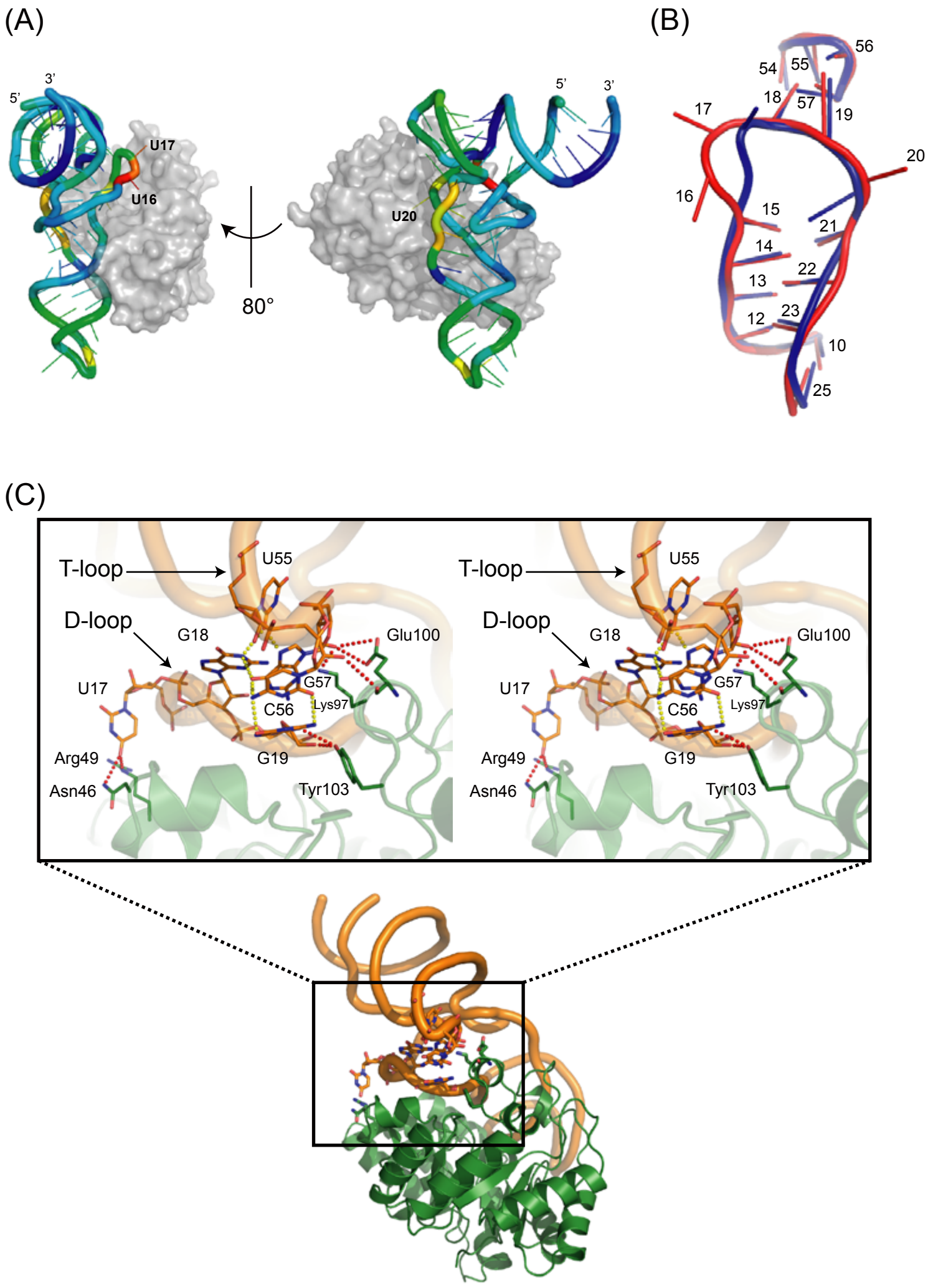
(A)
3'
5'
U17
U16
5'
3'
U20
80°
(B)
56
54
55
18
57
19
17
20
16
15
21
14
22
13
23
12
10
25
(C)
T-loop
U55
D-loop
G18
Glu100
U17
G57
C56
Lys97
Arg49
G19
Asn46
Tyr103
T-loop
U55
D-loop
G18
Glu100
U17
G57
C56
Lys97
Arg49
G19
Asn46
Tyr103

Figure 2

(A)

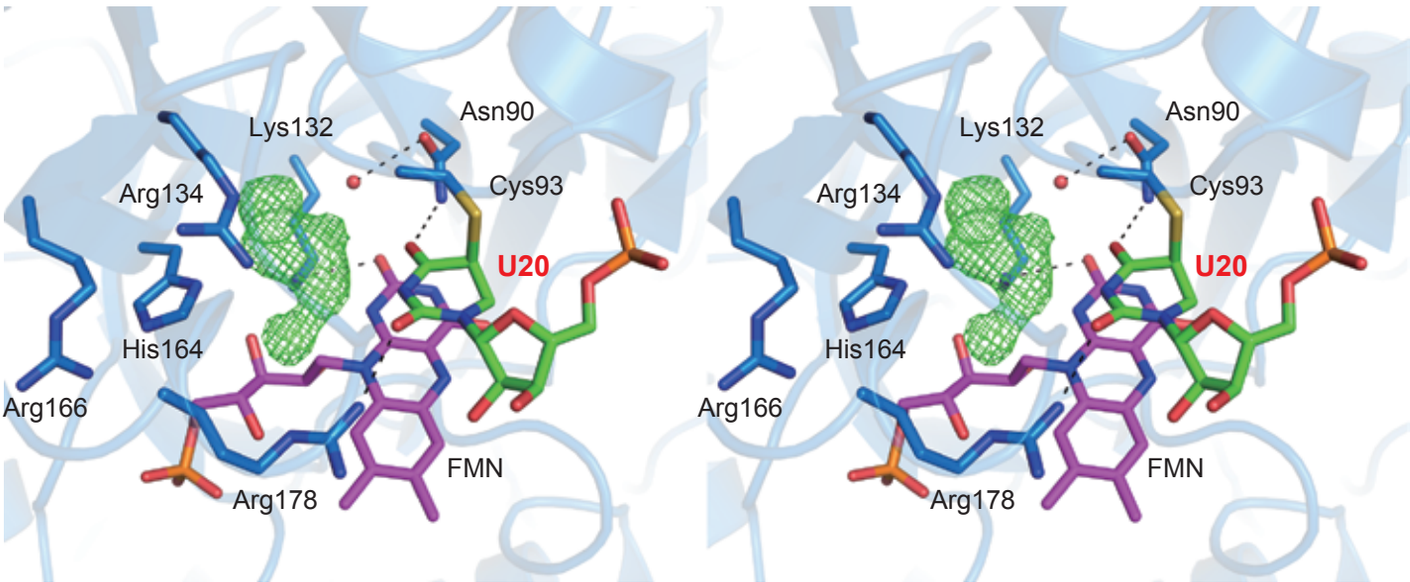
Lys132
Asn90
Arg134
Cys93
U20
His164
Arg166
FMN
Arg178
Lys132
Asn90
Arg134
Cys93
U20
His164
Arg166
FMN
Arg178

(B)

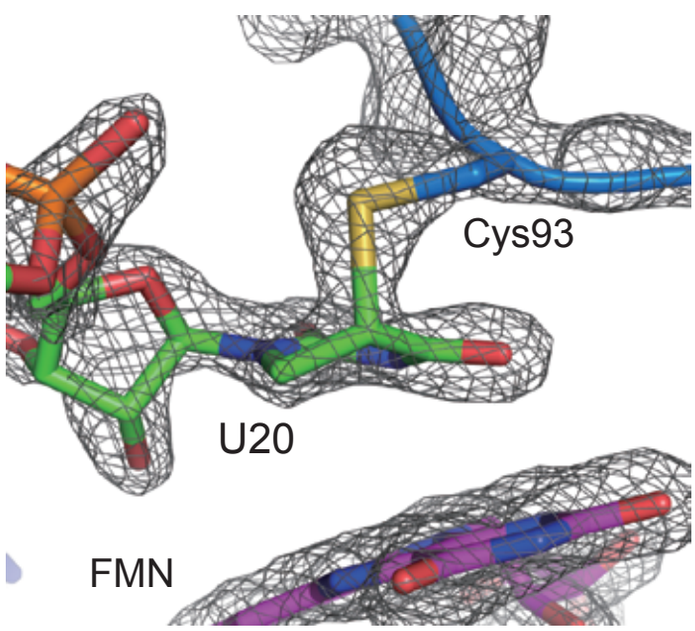
Cys93
U20
FMN

Figure 3

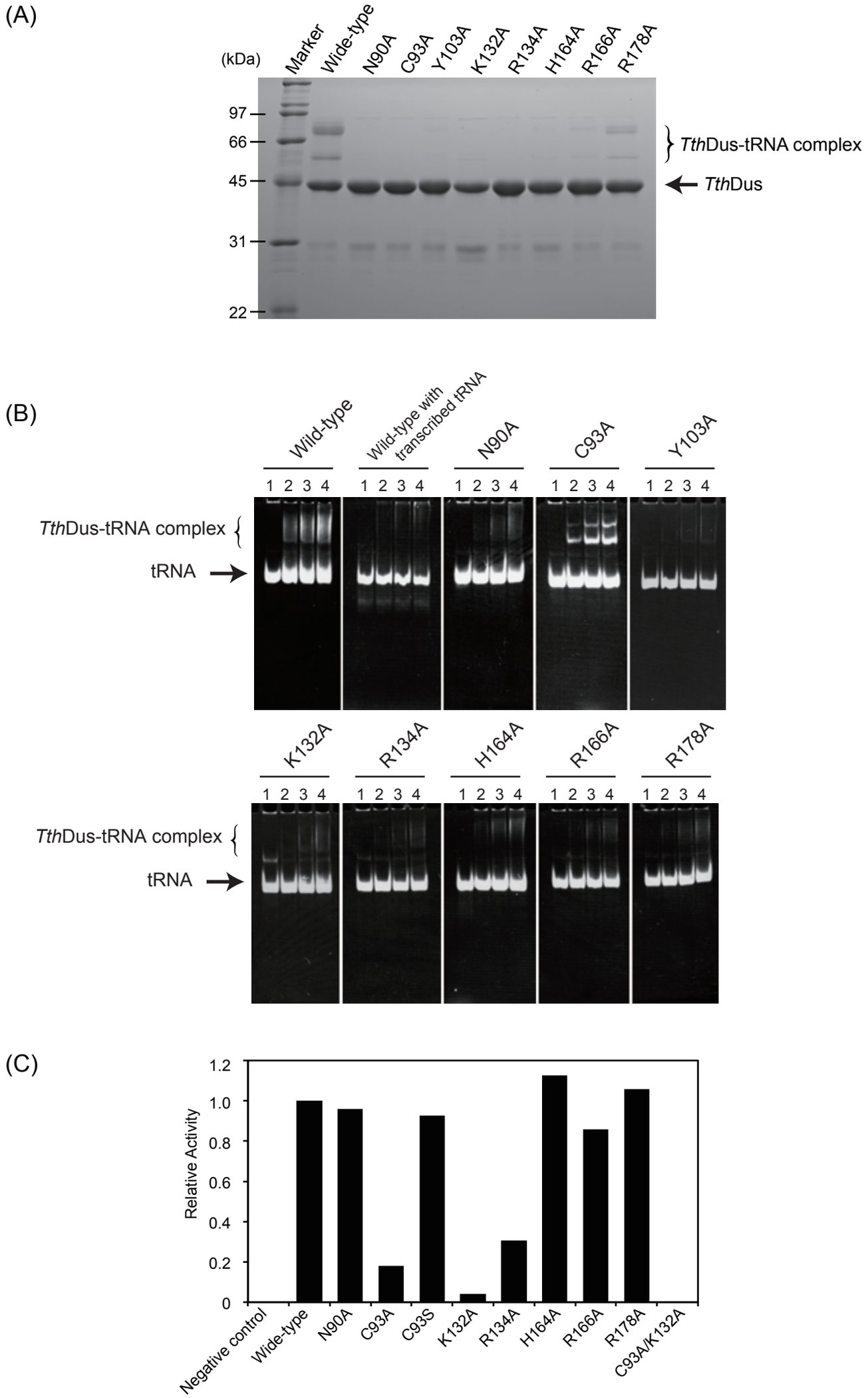
(A)
(kDa)
Marker
Wide-type
N90A
C93A
Y103A
K132A
R134A
H164A
R166A
R178A
97
66
45
31
22
TthDus-tRNA complex
TthDus
(B)
Wild-type
Wild-type with transcribed tRNA
N90A
C93A
Y103A
1 2 3 4
TthDus-tRNA complex
tRNA
K132A
R134A
H164A
R166A
R178A
(C)
Relative Activity
1.2
1.0
0.8
0.6
0.4
0.2
0
Negative control
Wide-type
N90A
C93A
C93S
K132A
R134A
H164A
R166A
R178A
C93A/K132A

Figure 4

(A)

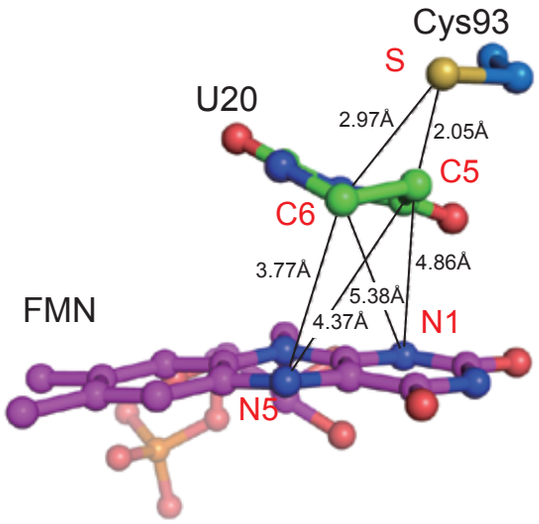
Cys93
S
U20
2.97Å
2.05Å
C5
C6
3.77Å
4.86Å
5.38Å
4.37Å
FMN
N1
N5

(B)

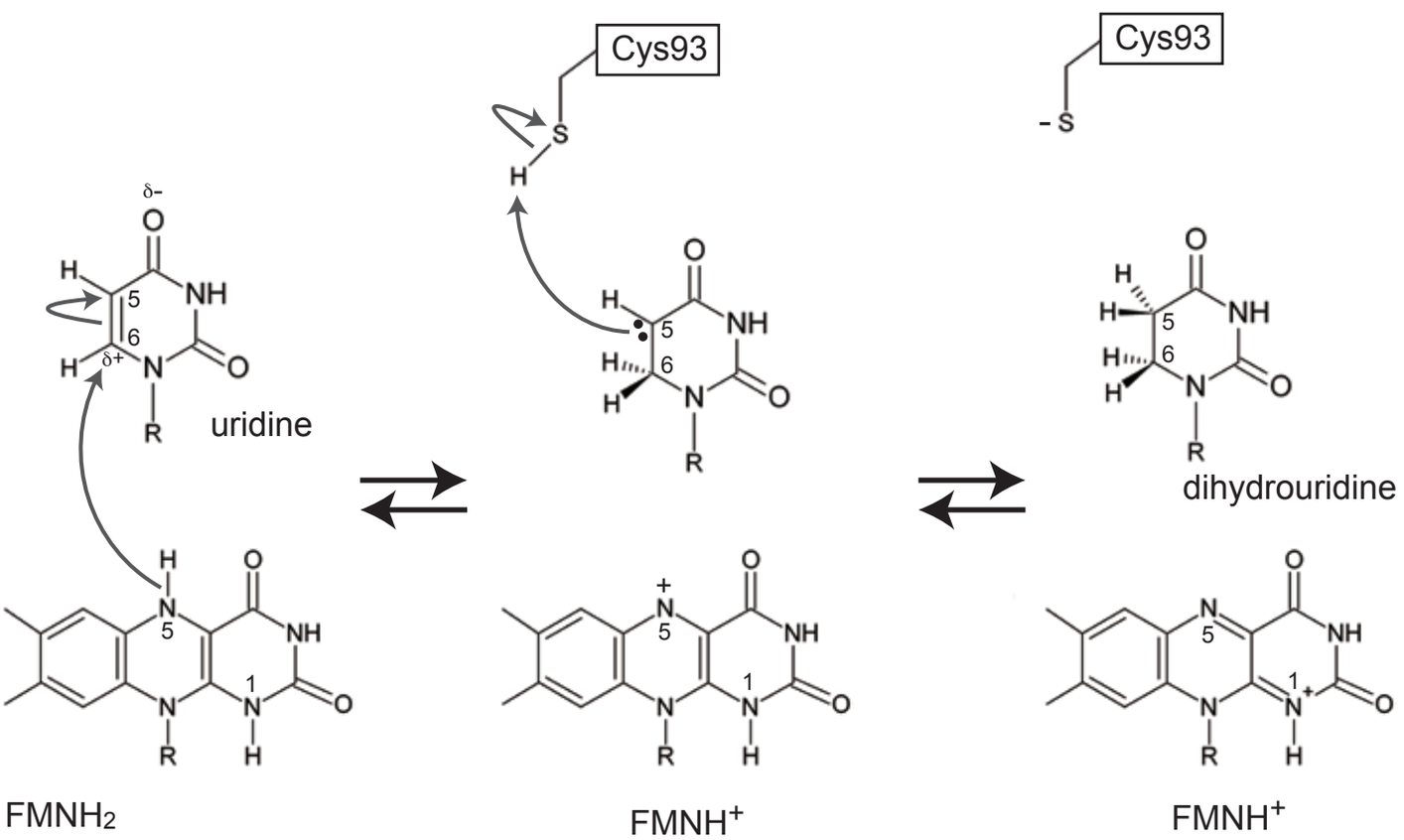
Cys93
Cys93
uridine
dihydrouridine
FMNH2
FMNH+
FMNH+

Figure 5